PCCP

PAPER

View Article Online
View Journal | View Issue

Cite this: *Phys. Chem. Chem. Phys.*, 2016, **18**, 11474

Giant strain geared to transformable H-bonded network in compressed β-D-mannose†

Ewa Patyk, Anna Jenczak and Andrzej Katrusiak*

Received 25th February 2016,
Accepted 17th March 2016

DOI: 10.1039/c6cp01286h

www.rsc.org/pccp

Networks of OH···O bonds in sugars and H_2O ices are hardly affected by temperature, but transform under pressure. Such a transition at 1.95 GPa in β-D-mannose induces strong strain, non-destructive for the single crystal and easily visible in its shape deformation. This transition occurs at the lowest pressure of all sugars investigated at high pressure so far. The giant strain propagates perpendicular to the clearly visible zero-strain planes. The transition reconstructs the 3-dimensional pattern of OH···O hydrogen bonds, changes the conformation of molecules and preserves the space-group symmetry, like the analogous transitions of α-D-glucose and D-sucrose. However, new repulsing O···O contacts have been generated at high pressure in D-mannose only.

Introduction

Hydrogen bonds and their transformations are immanent parts of biological systems and life processes at the molecular level.[1,2] Equally important are hydrogen bonds for geology and properties of rocks, as the minerals in Earth's crust contain more water than all seas and oceans.[3,4] The immense pressure in the deep-crust deposits strongly distorts the structure of minerals and most of all their softest interactions, including the hydrogen bonds.[5,6] Therefore, an understanding of the pressure effects on the hydrogen bonds is important. This information about H-bond transformations is also essential for designing new functional materials,[7] such as ferroelectrics and relaxors[8–10] for electronic applications, as well as for obtaining new polymorphs of pharmaceutical active ingredients.[11–14] It was shown recently that pressure significantly modifies the 3-dimensional OH···O bond motifs of D-sucrose and α-D-glucose.[15,16] In this respect sugars resemble the structures of H_2O ices, similarly governed by OH···O bonds building the frameworks, hardly affected by temperature, but efficiently destabilized by pressure.[17–20] However, in contrast to H_2O ices, it is characteristic that high-pressure transitions of D-sucrose, at 4.8 GPa, and α-D-glucose, at 5.4 GPa, preserve their space-group symmetry and lattice translations, an occurrence encountered at high pressure for quite a few compounds.[21–25] Presently, we found that a much lower pressure induces an exceptionally strong transformation between Phases I and II of β-D-mannose. Such major microscopic changes may lead to notable macroscopic effects.[26,27] The giant strain in the transforming D-mannose crystal is clearly visible under the microscope (Fig. 1).

D-Mannose, a close isomer of D-glucose, in its metabolism significantly differs from other sugars, mainly the energy carriers.

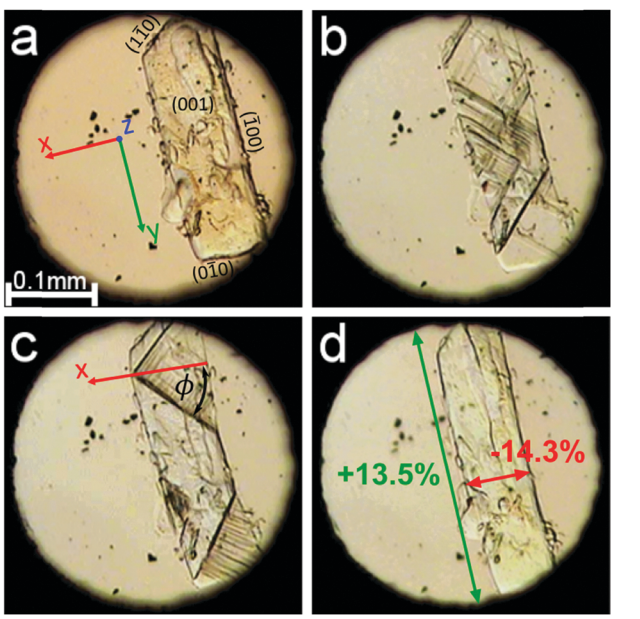

Fig. 1 Single crystal of β-D-mannose in Phase I (a); transformation (b and c) to the single crystal of Phase II (d), shown in 4 clips from Movie S1 (ESI,† see also Movies S2–S4 showing the transformation of other samples). The size changes between Phases I and II along the crystal directions [*x*] and [*y*] are marked in red and green, respectively. The crystal axes and Miller indices of selected faces are indicated in plate (a). Angle ϕ, between the direction of zero strain and the ***x*** axis calculated according to eqn (1) in the text, is marked in plate (c). Small ruby chips for pressure calibration are scattered in the DAC chamber.

Department of Materials Chemistry, Faculty of Chemistry, Adam Mickiewicz University, Umultowska 89b, Poznań, Poland. E-mail: katran@amu.edu.pl

† Electronic supplementary information (ESI) available: Detailed experimental and structural data; detailed information about intermolecular interactions; and multimedia files illustrating crystal shape changes. CCDC 1450799–1450809. For ESI and crystallographic data in CIF or other electronic format see DOI: 10.1039/c6cp01286h

Metabolized D-mannose is incorporated into glycolipids and glycoproteins, so its role is mainly structural.[28] Moreover, it exhibits antibacterial and antiviral properties, hence, it is used to treat and prevent recurrent urinary tract infections.[29,30] Owing to the slower absorption compared to other sugars, D-mannose travels in blood to the urinary tract, where it binds competitively to *Escherichia coli* bacteria, preventing their adhesion to mucous membranes and leading to their efficient excretion.[31] For these and other reasons D-mannose is an important active pharmaceutical ingredient (API) often described as a healing sugar.[32] The considerably different metabolism of D-mannose and D-glucose results from their different codes of H-donor and H-acceptor hydroxyl groups,[33] convertible conformation and intermolecular interactions[34] adjusting to various environments.[35] The structure of the β-anomer of D-mannose crystals, despite its diverse applications,[29,30] has remained unknown until now.

Experimental

A single crystal of β-D-mannose (analytical grade; from VEB Berlin-Chemie) was installed in a modified Merrill-Bassett diamond-anvil cell (DAC).[36] The gasket was made of 0.3 mm tungsten foil with a spark-eroded hole, 0.3–0.4 mm in diameter. The sample position in the DAC chamber was fixed with a few cellulose fibers or a small amount of glue. Ethanol solution saturated with D-mannose, fluorinert or an *n*-pentane : isopentane (vol 1 : 1) mixture was used as hydrostatic medium. Pressure inside the DAC was measured according to the ruby fluorescence method[37] using an enhanced Photon Control Inc. spectrometer, affording an accuracy of 0.02 GPa. Diffraction data were collected at 0.48, 1.00, 1.60, 1.90, 2.02, 2.10 and 2.35 GPa (Fig. S1, ESI†) on a four-cycle KUMA KM4-CCD X-ray diffractometer using graphite monochromated MoKα radiation, and at 2.85 GPa using a 4-cycle Xcalibur diffractometer equipped with the EOS CCD detector and an AgKα radiation source. The crystal and DAC centering were performed according to the methods described previously.[38] Low-temperature data (150–295 K range; Fig. S2, ESI†) were measured using a 4-circle SuperNova diffractometer, CuKα radiation, and an Oxford Cryosystems attachment. For data collection, UB-matrix determination, absorption correction and data reduction, the program CrysAlisPro[39] was used. The crystal structures were solved by direct methods using SHELXS[40] and refined with the program SHELXL.[41] Hydrogen atoms were located by molecular geometry with U_{iso} equal to $1.2U_{eq}$ for C-carriers and $1.5U_{eq}$ for O-carriers, and with the O–H and C–H bond lengths fixed at the distances of 0.82 Å for oxygen atoms, and 0.98 or 0.97 Å for tertiary and secondary carbon atoms, respectively. To allow the gradual transformation of the sample between the phases and the recording of the visual changes in the β-D-mannose crystal shape (Fig. 1, Movies S1–S4, ESI†), a membrane DXR-GM DAC from Diacell was applied for fine-tuning the pressure through the phase transition.

We found that β-D-mannose is compressed monotonically up to 1.95(2) GPa, when it undergoes a phase transition. It retains the symmetry of the orthorhombic space group $P2_12_12_1$ and such phase transitions are described as *isostructural*, *isomorphic*, and sometimes as *isosymmetric*.[21] Crystallographic data for β-D-mannose in ambient and high-pressure phases are compared in Table 1 (*cf.* Tables S1 and S2 in the ESI†) CCDC 1450799–1450809.

Table 1 Selected structural data for β-D-mannose Phases I and II at the pressure limits of their stability regions and at 2.85 GPa, all at 295 K (*cf.* Tables S1 and S2 in the ESI)

$C_6H_{12}O_6$	Phase I	Phase I	Phase II	Phase II
Pressure (GPa)	0.0001	1.90(2)	2.02(2)	2.85(2)
Crystal system	Orthorhombic		Orthorhombic	
Space group	$P2_12_12_1$	$P2_12_12_1$	$P2_12_12_1$	$P2_12_12_1$
a (Å)	5.6684(2)	5.375(18)	4.609(3)	4.5744(6)
b (Å)	7.5720(2)	7.436(4)	8.438(6)	8.386(3)
c (Å)	18.1425(5)	17.849(8)	17.40(9)	17.212(16)
Volume (Å^3)	778.69(4)	713(2)	677(3)	660.3(6)
Z	4	4	4	4
D_x (g cm^{-3})	1.537	1.678	1.768	1.812
Final R_1 ($I > 4\sigma_I$)	0.0334	0.0723	0.0725	0.0718

Compressibility parameters $\beta_x = -1/x\partial x/\partial p$, where *x* represents the measured unit-cell dimensions *V*, *a*, *b*, and *c*, have been fitted with quadratic polynomials for Phase I and the exponential decay function for Phase II (Table S7, ESI†). Intermolecular interactions have been analysed for the structures with C–H and O–H bonds normalized to the neutron-determined distances of 0.97 Å for oxygen atoms, and, respectively, 1.098 and 1.091 Å for tertiary and secondary carbon atoms, according to Allen and Bruno.[42] Contacts have been classified as hydrogen bonds OH···O for O···O distances shorter than 3.04 Å (*i.e.* the sum of van der Waals radii[43]); as CH···O bonds for H···O distances shorter than 2.72 Å and for the C–H···O angle higher than 110°;[43,44] and as H···H contacts for distances shorter than 2.4 Å.[43]

Results and discussion

The giant strain between β-D-mannose Phases I and II, the largest ever recorded for sugars, allows the clear visual observation of the transformation fronts, passing through the crystal (Fig. 1).

The transition abruptly reduces the crystal volume by nearly 4% (Fig. 2). This transition strongly rearranges hydrogen bonds OH···O, and changes the molecular aggregation. In Phase I each molecule is the H-donor in five OH···O bonds and the H-acceptor in five H-bonds, and in Phase II seven independent OH···O bonds are formed, as illustrated in Fig. 3. The changes in the H-bonding pattern at 1.95 GPa are: (i) the bond O1H···O3^{3645} is broken and in its place the bond O1H···O6^{3655} is formed; (ii) the bond O2H···O5^{3655} bifurcates[45] to the oxygen atom O1^{3655}; (iii) the bond O3H···O4^{4565} reverses its polarization to O3···HO4^{4565}, while the hydroxyl group O3H forms a bifurcated H-bond with atoms O3^{4465} and O4^{4465}; (vi) from the broken O4H···O6^{4555} bond hydroxyl O4H is redirected to the reversed bond O4H···O3^{4465}; and the hydroxyl O6H remains in the ambient–pressure bond O6H···O1^{3545}.

It is noteworthy, that ten hydrogen bonds OH···O per each β-mannose molecule in Phase I form a 3-dimensional supramolecular network of multitude of interconnected rings and chains/helices.[15] The network of 14 OH···O bonds per molecule in Phase II is even more complex. The unequivocal description

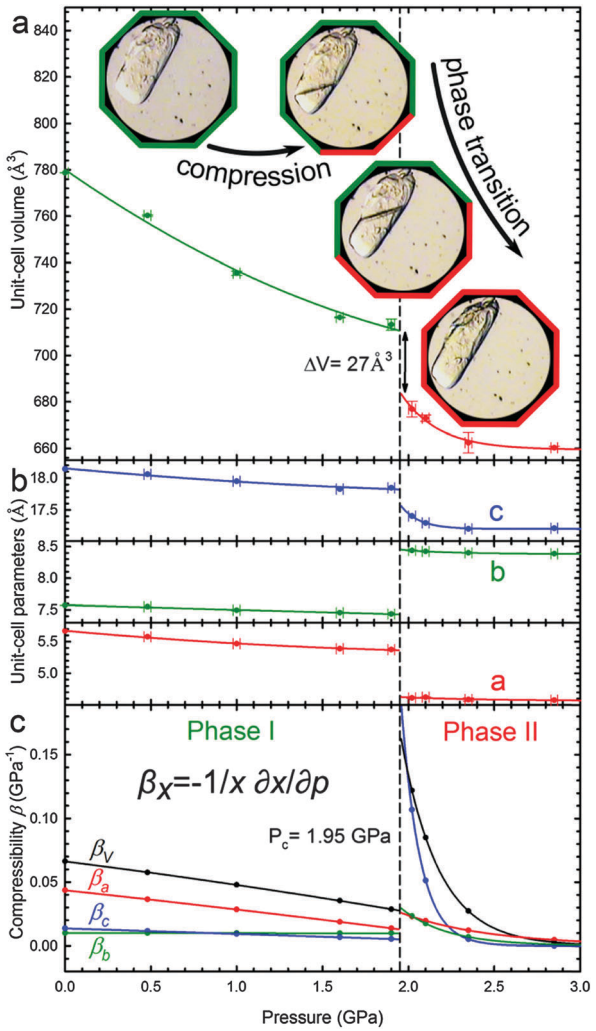

Fig. 2 Pressure dependence of β-D-mannose (a) the unit-cell volume (Phases I and II marked in green and red, respectively); (b) unit-cell parameters; as well as (c) compressibilities β_x calculated for $x = a, b, c$ and V (Table S8, ESI†). Critical pressure P_c of the phase transition is marked by the vertical dashed line. The insets show a sample in Phases I (green octagonal rim) and II (red), as well as for the transforming stages (green/red).

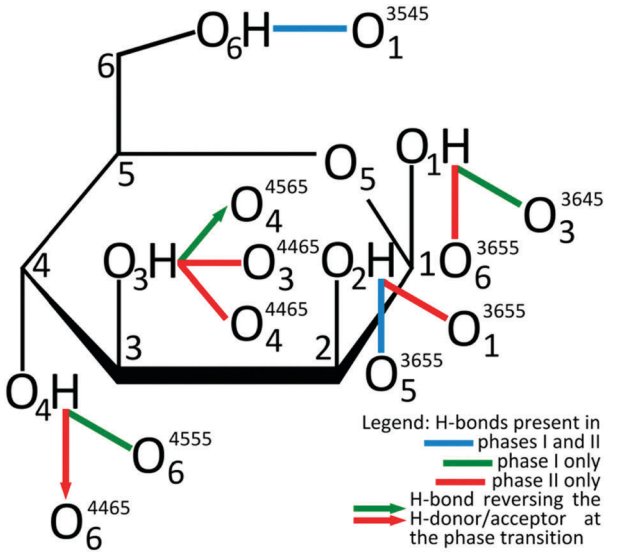

Fig. 3 Transformation of OH···O hydrogen bonds between β-D-mannose Phases I and II schematically charted for H-donor groups onto Fisher's formula, complemented with H-accepting oxygen atoms, according to the legend below the drawing. ORTEP symmetry codes[47] are explicitly listed in Table S3 (ESI†).

of these networks exceeds the capabilities of graph descriptors used for the H-bonding patterns.[46] Therefore we have applied the rigorous ORTEP symmetry codes for precisely describing the H-bonds of one molecule in its nearest vicinity. The symmetry transformations described in superscripts by 4-digit ORTEP codes[47] are explicitly listed in Table S3 (ESI†).

The extent of the transformations in the OH···O bonding network is quantitatively illustrated in Fig. 4, where the O···O and H···O distances of all H-bonds present either in Phase I or II are plotted. The transition considerably changes the distances of intermolecular O···O contacts, even by more than 2 Å for the H-bonds O1H···O6^{3655} and O3H···O3^{4465} formed in Phase II. The shortest of contacts O···O and H···O are only compressed from 2.70 Å to 2.56 Å and from 1.80 Å to 1.67 Å, respectively. High pressure slightly reduces the C···O distances, however the shortest of (C)H···O contacts in Phase II are longer than those in Phase I (Fig. S8 in the ESI†). In this respect the shortest OH···O and CH···O bonds behave differently than in the pressure-transformed sucrose and glucose, where in Phase II the O···O distances are somewhat longer and CH···O bonds shorter than before the transition in Phase I. However, it is a common feature of the β-mannose, sucrose and glucose structures that the excess of H-acceptor sites (general for sugars) at high pressure is balanced by the formation of bifurcated OH···O bonds and new CH···O bonds.

The shortest of H···H contacts in Phase II is only about 0.3 Å shorter than that in Phase I, and this compression is stronger than that observed for the other types of contacts (Fig. S11, ESI†). All dimensions of intermolecular contacts (Fig. 4 and Fig. S4–S11, ESI†) are consistent with the strong molecular rearrangement and compression of the structure. The reduction of H···H distances is consistent with the collapse of the small voids in Phase I. The voids are contained between the molecules arranged in a herringbone pattern in Phase I, while above 1.95 GPa the molecules are nearly parallel along the plane (***bc***), as can be seen in the structures and their schemes in Fig. 5. To accommodate these molecular rotations, the crystal shrinks along ***a*** and expands along ***b***. Moreover, the longest dimension of the molecule between atoms O2 and O6 becomes better aligned along ***b*** within the (***bc***) plane just above the transition, which is consistent with the more pronounced compression of the crystal along ***c*** and expansion along ***b***.

The considerable volume collapse at P_c allows the transition in β-mannose to be induced in gradually increasing portions of the sample crystal by a very slow increase in the volume reduction of the DAC chamber. In principle, if all the sample volume V_s collapses by ΔV_s at P_c, then the reduction of the volume of the DAC chamber by ΔV_s from the start of the transition does not increase the pressure in the DAC until the entire sample has

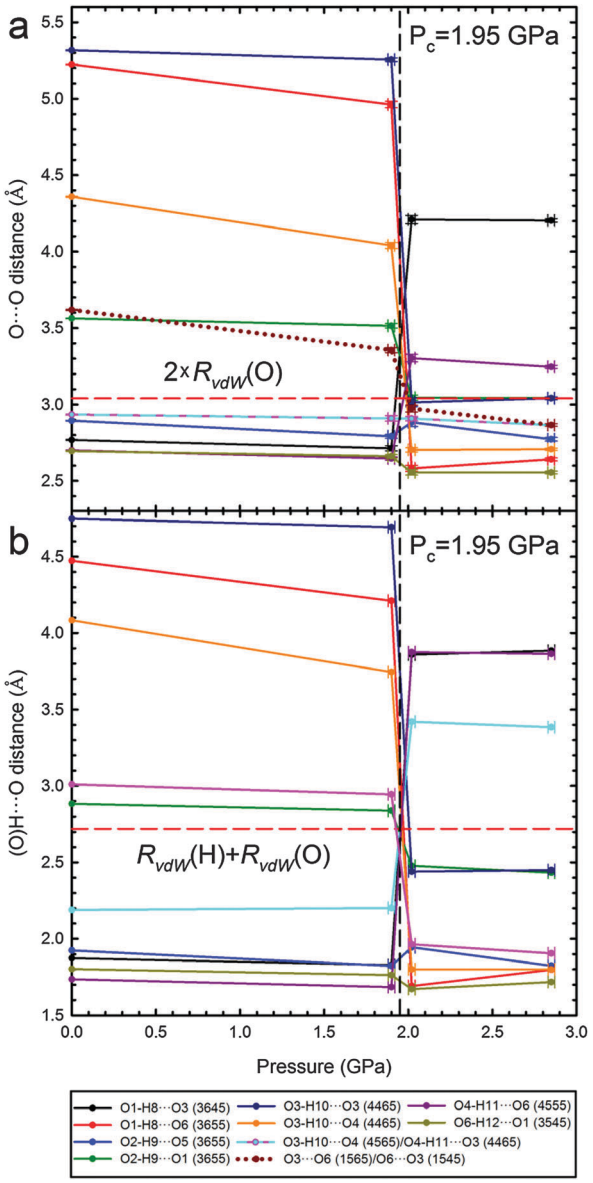

Fig. 4 Pressure dependence of O···O (a) and H···O (b) short distances present either in β-D-mannose Phase I or II (*cf.* Table S4, ESI†). Lines joining points are only for guiding the eye. Horizontal red dashed lines indicate the sum of van der Waals radii (R_{vdW}) O···O (3.04 Å) and H···O (2.72 Å).[43]

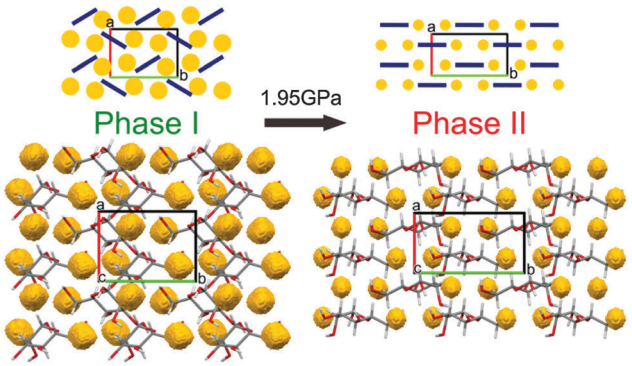

Fig. 5 Molecular arrangement in β-D-mannose Phase I at 1.90(2) GPa and Phase II at 2.02(2) GPa viewed along the direction [001].[48] Structural voids, calculated using program Mercury[48] for the probe radius 0.7 Å and the grid spacing 0.1 Å, are marked in yellow. For clarity, the overlapping molecules have been omitted. In the schematic drawings (top), molecules are represented by navy-blue bars and structural voids by yellow circles.

transformed (Fig. 2a). This feature illustrates the possible applications of such materials for shock-absorbing or stress-compensating devices, but it also allows observations of the transition front propagating through the sample (Fig. 1).

It is remarkable that the giant strain in the β-mannose crystal does not break the sample. This infers that the transition front proceeds along the planes that minimize the local strain. It can be seen in Fig. 1 that the transition fronts only approximately progress along crystal planes (±1 ±1 0). For the crystal exhibiting negative linear compressibility, such as β-mannose, there are directions of zero strain and these directions can be calculated from the strain tensor between Phases I and II at P_c. For the transition in β-mannose the strongest strain is generated within the (***ab***) plane, due to the strongest positive and negative linear compression of the crystal along ***a*** and ***b***, respectively, (Fig. 1). Owing to the coexistence of positive and negative linear compression within the (***ab***) plane, there are directions of zero strain along the planes parallel to (***c***) and inclined to axis ***a*** by angle ϕ

$$\phi = \pm tg^{-1}[(1 - a_{II}^2/a_I^2)/(b_{II}^2/b_I^2 - 1)]^{1/2}, \qquad (1)$$

where indices in unit-cell dimensions a_I, b_I, a_{II} and b_{II} refer to Phases I and II, respectively. For the zero-strain transition fronts parallel to the ***c*** axis, the ϕ angle calculated in this way is 43.83°, in accordance with the microscopic visual observations (*cf.* Fig. 1 and Movies S1–S4 in the ESI†).

Conclusions

The high-pressure effects in β-D-mannose strikingly resemble those in D-sucrose and α-D-glucose. In all these systems, crystals transform with no space-group symmetry change, when the OH···O bonding network reconstructs to a tighter version, with more bifurcated OH···O bonds and more CH···O bonds compensating for the insufficient number of hydroxyl donors. The transition in β-D-mannose, occurring at considerably lower pressure than those in D-sucrose and α-D-glucose, induces a giant anomalous strain, which is coupled to the molecular rearrangement. It appears that the sophisticated geometric code of H-donors and H-acceptors in sugars controls the monotonic and discontinuous strain in the compressed crystals. The experimental measurements of crystal compression are presently available for three sugars only, however it is already an intriguing result that each of these sugars undergoes only one isostructural phase transition in the high-pressure range, where several phase transitions occur for the H_2O ices, built of considerably simpler and more symmetric (C_{2v}) molecules. It shows that the small H_2O molecules cannot control the crystal symmetry and directions of crystal transformations in such a precise and unique way as the much more complex molecules of sugars. This conclusion

is partly supported by the relatively scarce occurrence of polymorphs in sugars, reported—aside from the high-pressure transformations in α-D-glucose, β-D-mannose, and D-sucrose—for D-ribose,[49] β-D-allose,[50,51] lactose,[52,53] α,α-trehalose[54,55] and cellulose.[56] Clearly, further studies are needed for the better understanding of external-stimuli effects and functional responses of H-bonded networks, which will ultimately allow their rational control and applications.

Acknowledgements

We are grateful to Ms Michalina Anioła and Wielkopolska Center of Advanced Technologies for the experimental support, as well as to Mr Michał Andrzejewski and Mr Michał Kaźmierczak for their assistance in recording and editing movies included in the ESI.†

Notes and references

1 G. A. Jeffrey and W. Saenger, *Hydrogen Bonding in Biological Structures*, Springer, Berlin, Heidelberg, 1994, ch. 1, pp. 3–14, ch. 19, pp. 351–393.
2 G. R. Desiraju and T. Steiner, *The Weak Hydrogen Bond: In Structural Chemistry and Biology*, Oxford University Press, Oxford, 2001, ch. 5, pp. 343–440.
3 B. Schmandt, S. D. Jacobsen, T. W. Becker, Z. Liu and K. G. Dueker, *Science*, 2014, **344**, 1265.
4 D. G. Pearson, F. E. Brenker, F. Nestola, J. McNeill, L. Nasdala, M. T. Hutchison, S. Matveev, K. Mather, G. Silversmit, S. Schmitz, B. Vekemans and L. Vincze, *Nature*, 2014, **507**, 221.
5 N. Noguchi, T. Moriwaki, Y. Ikemoto and K. Shinoda, *Am. Mineral.*, 2012, **97**, 134.
6 P. F. Zanazzi, M. Montagnoli, S. Nazzareni and P. Comodi, *Am. Mineral.*, 2007, **92**, 655.
7 G. Resnati, E. Boldyreva, P. Bombicz and M. Kawano, *IUCrJ*, 2015, **2**, 675.
8 L. Kong, L. Wang, S. Zhang, O. Tschauner, Y. Zhao, W. Yang, H. Liu and H.-K. Mao, *Appl. Phys. Lett.*, 2012, **101**, 062904.
9 T. Aoyama, K. Yamauchi, A. Iyama, S. Picozzi, K. Shimizu and T. Kimura, *Nat. Commun.*, 2014, **5**, 4927.
10 M. Szafrański, *CrystEngComm*, 2014, **16**, 6250.
11 F. P. A. Fabbiani, G. Buth, D. C. Levendis and A. J. Cruz-Cabeza, *Chem. Commun.*, 2014, **50**, 1817.
12 F. P. A. Fabbiani, D. R. Allan, W. I. F. David, A. J. Davidson, A. R. Lennie, S. Parsons, C. R. Pulham and J. E. Warren, *Cryst. Growth Des.*, 2007, **7**, 1115.
13 M. A. Neumann, J. van de Streek, F. P. A. Fabbiani, P. Hidber and O. Grassmann, *Nat. Commun.*, 2015, **6**, 7793.
14 E. V. Boldyreva, T. P. Shakhtshneider, H. Ahsbahs, H. Sowa and H. Uchtmann, *J. Therm. Anal. Calorim.*, 2002, **68**, 437.
15 E. Patyk, J. Skumiel, M. Podsiadło and A. Katrusiak, *Angew. Chem., Int. Ed.*, 2012, **51**, 2146.
16 E. Patyk and A. Katrusiak, *Chem. Sci.*, 2015, **6**, 1991.
17 C. G. Salzmann, P. G. Radaelli, B. Slater and J. L. Finney, *Phys. Chem. Chem. Phys.*, 2011, **13**, 18468.
18 B. Kamb and B. L. Davis, *Proc. Natl. Acad. Sci. U. S. A.*, 1964, **52**, 1433.
19 J. D. Londono, W. F. Kuhs and J. L. Finney, *J. Chem. Phys.*, 1993, **98**, 4878.
20 R. J. Hemley, A. P. Jephcoat, H. K. Mao, C. S. Zha, L. W. Finger and D. E. Cox, *Nature*, 1987, **330**, 737.
21 A. Jayaraman, *Phys. Rev.*, 1965, **137**, A179; K. Gesi, *Phase Transitions*, 1992, **40**, 187; A. G. Christy, *Acta Crystallogr., Sect. B: Struct. Sci.*, 1995, **51**, 753.
22 W. Cai and A. Katrusiak, *Nat. Commun.*, 2014, **5**, 4337.
23 D. Paliwoda, K. Kowalska, M. Hanfland and A. Katrusiak, *J. Phys. Chem. Lett.*, 2013, **4**, 4032.
24 J. Zhao, L. Wang, D. Dong, Z. Liu, H. Liu, G. Chen, D. Wu, J. Luo, N. Wang, Y. Yu, C. Jin and Q. Guo, *J. Am. Chem. Soc.*, 2008, **130**, 13828.
25 S. V. Goryainov, E. V. Boldyreva, M. B. Smirnov, H. Ahsbahs, V. V. Chernyshev and H.-P. Weber, *Dokl. Phys. Chem.*, 2003, **390**, 154.
26 Ž. Skoko, S. Zamir, P. Naumov and J. Bernstein, *J. Am. Chem. Soc.*, 2010, **132**, 14191.
27 M. Lusi and J. Bernstein, *Chem. Commun.*, 2013, **49**, 9293.
28 R. H. Herman, *Am. J. Clin. Nutr.*, 1971, **24**, 488.
29 B. Kranjčec, D. Papeš and S. Altarac, *World J. Urol.*, 2014, **32**, 79.
30 D. Porru, A. Parmigiani, C. Tinelli, D. Barletta, D. Choussos, C. Di Franco, V. Bobbi, S. Bassi, O. Miller, B. Gardella, R. E. Nappi, A. Spinillo and B. Rovereto, *J. Clin. Urol.*, 2014, **7**, 208.
31 S. Vanwetswinkel, A. N. Volkov, Y. G. J. Sterckx, A. Garcia-Pino, L. Buts, W. F. Vranken, J. Bouckaert, R. Roy, L. Wyns and N. A. J. Van Nuland, *J. Med. Chem.*, 2014, **57**, 1416.
32 E. I. Mondoa, *Sugars That Heal: The New Healing Science of Glyconutrients*, Random House Publishing Group, New York, 2008, ch. 2, pp. 20–37.
33 K. H. Nam, M. W. Sung and K. Y. Hwang, *Biochem. Biophys. Res. Commun.*, 2010, **391**, 1131.
34 T. Tomašić, S. Rabbani, M. Gobec, I. M. Raščan, Č. Podlipnik, B. Ernst and M. Anderluh, *MedChemComm*, 2014, **5**, 1247.
35 J. F. Nagle, M. Mille and H. J. Morowitz, *J. Chem. Phys.*, 1980, **72**, 3959.
36 L. Merrill and W. A. Bassett, *Rev. Sci. Instrum.*, 1974, **45**, 290–294.
37 H. K. Mao, J. Xu and P. M. Bell, *J. Geophys. Res.: Solid Earth*, 1986, **91**, 4673.
38 A. Budzianowski and A. Katrusiak, in *High-Pressure Crystallography*, ed. A. Katrusiak and P. McMillan, Springer, Netherlands, 2004, pp. 101–112.
39 Oxford Diffraction, Oxford Diffraction Ltd., Xcalibur CCD system, CrysAlis Software system, Version 1.171, 2004.
40 G. M. Sheldrick, *Acta Crystallogr., Sect. A: Found. Crystallogr.*, 2008, **64**, 112.
41 G. M. Sheldrick, *Acta Crystallogr., Sect. C: Struct. Chem.*, 2015, **71**, 3.
42 F. H. Allen and I. J. Bruno, *Acta Crystallogr., Sect. B: Struct. Sci.*, 2010, **66**, 380.
43 A. Bondi, *J. Phys. Chem.*, 1964, **68**, 441.

44 E. Arunan, G. R. Desiraju, R. A. Klein, J. Sadlej, S. Scheiner, I. Alkorta, D. C. Clary, R. H. Crabtree, J. J. Dannenberg, P. Hobza, H. G. Kjaergaard, A. C. Legon, B. Mennucci and D. J. Nesbitt, *Pure Appl. Chem.*, 2011, **83**, 1637.
45 G. A. Jeffrey and S. Takagi, *Acc. Chem. Res.*, 1978, **11**, 264.
46 M. C. Etter, J. C. MacDonald and J. Bernstein, *Acta Crystallogr., Sect. B: Struct. Sci.*, 1990, **46**, 256.
47 C. K. Johnson, ORTEPII. Report ORNL-5138, TN: Oak Ridge National Laboratory, Memphis, 1976.
48 C. F. Macrae, I. J. Bruno, J. A. Chisholm, P. R. Edgington, P. McCabe, E. Pidcock, L. Rodriguez-Monge, R. Taylor, J. van de Streek and P. A. Wood, *J. Appl. Crystallogr.*, 2008, **41**, 466.
49 D. Šišak, L. B. McCusker, G. Zandomeneghi, B. H. Meier, D. Bläser, R. Boese, W. B. Schweizer, R. Gilmour and J. D. Dunitz, *Angew. Chem., Int. Ed.*, 2010, **49**, 4503.
50 L. M. J. Kroon-Batenburg, P. van der Sluis and J. A. Kanters, *Acta Crystallogr., Sect. C: Cryst. Struct. Commun.*, 1984, **40**, 1863.
51 P. A. Bonnet, J. van de Streek, A. V. Trask, W. D. S. Motherwell and W. Jones, *CrystEngComm*, 2004, **6**, 535.
52 C. Platteau, J. Lefebvre, F. Affouard and P. Derollez, *Acta Crystallogr., Sect. B: Struct. Sci.*, 2004, **60**, 453.
53 C. Platteau, J. Lefebvre, F. Affouard, J.-F. Willart, P. Derollez and F. Mallet, *Acta Crystallogr., Sect. B: Struct. Sci.*, 2005, **61**, 185.
54 G. A. Jeffrey and R. Nanni, *Carbohydr. Res.*, 1985, **137**, 21.
55 H. Nagase, N. Ogawa, T. Endo, M. Shiro, H. Ueda and M. Sakurai, *J. Phys. Chem. B*, 2008, **112**, 9105.
56 A. Isogai, M. Usuda, T. Kato, T. Uryu and R. H. Atalla, *Macromolecules*, 1989, **22**, 3168.